Volume 10 | Number 7 | 7 April 2023

10 YEARS ANNIVERSARY

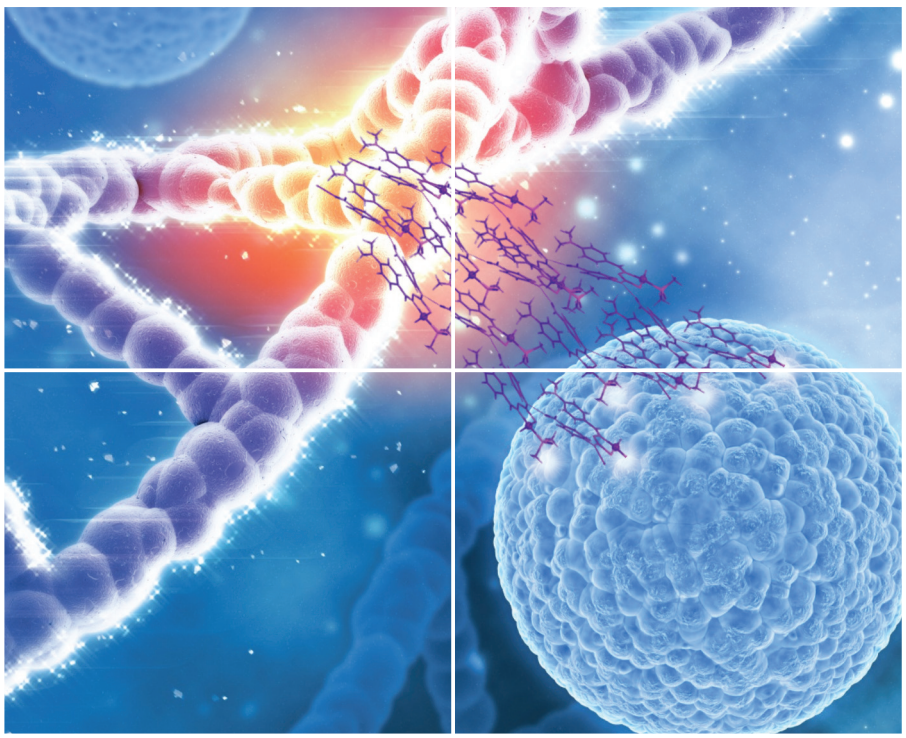

INORGANIC CHEMISTRY

FRONTIERS

CCS 中国化学会 CHINESE CHEMICAL SOCIETY

PEKING UNIVERSITY 1898

ROYAL SOCIETY OF CHEMISTRY

rsc.li/frontiers-inorganic

INORGANIC CHEMISTRY
FRONTIERS

RESEARCH ARTICLE

View Article Online
View Journal | View Issue

Cite this: *Inorg. Chem. Front.*, 2023, **10**, 1986

Two novel Pd thiosemicarbazone complexes as efficient and selective antitumoral drugs†

Tania Hidalgo, [a] David Fabra, [b] Raul Allende,‡[b] Ana I. Matesanz, [b] Patricia Horcajada, *[a] Tarita Biver *[c] and Adoracion G. Quiroga *[b]

Received 15th November 2022,
Accepted 14th December 2022

DOI: 10.1039/d2qi02424a

rsc.li/frontiers-inorganic

Cancer is a leading cause of death worldwide, accounting for nearly 10 million deaths in 2020. Palladium complexes can be used as anticancer and pharmacological agents as a promising alternative to overcome the disadvantages of platinum drugs, controlling the speciation in solution and limiting toxicity. In this study, two novel complexes were developed and their speciation in solution was deeply investigated, demonstrating their stability in solution together with their behavior *versus* nucleic acid models and serum proteins *via* thermodynamic studies. Furthermore, both complexes were demonstrated to be efficient and more specific than the benchmark cisplatin drug because of their lower toxicity to healthy cells.

1. Introduction

Cancer is likely to remain one of the biggest global health challenges in the 21st century, becoming the first leading cause of death for people aged 45–64 years. In 2020, 2.7 million people in the European Union (EU) were diagnosed with cancer, ~1.3 million people lost their lives, and an increase of 24% is expected by 2035 with an economic impact of €100 billion per year. Although the EU has been tackling cancer for decades, the need for a renewed commitment to cancer prevention, treatment and care is one of the main missions and actions for the European community (*e.g.*, Europe's Beating Cancer Plan),[1,2] where repurposing medicines to fight cancer is part of the plan, underpinning data sharing and collaborations.

Despite the therapeutic discoveries made so far, the side effects (*e.g.*, nausea; oto-, nephro-, hepato-toxicities) and treatment resistance to classical chemotherapeutic agents continue to be major drawbacks in cancer therapies, leading to higher inefficacies. The use of metals in cancer therapy has attracted a great deal of attention in recent years, such as in the case of cisplatin: despite its side effects, it is still one of the most successful anticancer compounds used clinically for diverse human cancers (ovarian, bladder, gastrointestinal, *etc.*).[3] Its mechanism of action involves the aquation of its chloride ligands, as Pt(II) complexes' geometry is labile to ligand exchange. Even though the monoaquo complex is the major species (the fast aquation), hydroxo species formation and, in general, speciation inside the cell contribute greatly to generating serious side effects. Therefore, novel approaches to pharmaceutic design are needed.

A recent tendency has focused on platinum group elements (Ru, Rh, Pd, *etc.*)[4–7] and, more precisely, palladium complexes since they display moderate antitumoral activity associated with reduced toxicological effects. In this case, their design is based on the similarity of the metal centre to the Pt(II) analogue (in terms of the electronic structure and coordination chemistry) with a remarkably higher lability. In addition, their cytotoxic activity is more favourable due to the enhanced stability provided by the strong ligand–metal coordination [*e.g.*, polydentate amines, carbamates, thiosemicarbazones (TSCN)], creating a chelating effect.[8] This effect drives their reactivity toward activation reactions and binding affinities, promoting their biomedical applications,[9–12] and, more importantly, might help to overcome the problem of their possible speciation. Bearing in mind all these promising features, the development of palladium complexes for clinical applications has lately been reinforced with many studies,[13] revealing their high potential therapeutic performance, especially against triple negative breast cancer (TNBC), chemotherapy-resistant cancers or photodynamic therapy resistant prostate cancers.[14] In this sense, some of us have actively participated by designing pharmacologically active TSCN to achieve a variety of efficient platinum and palladium mononuclear and polynuclear complexes.[15] A similar anticancer activity of both metals using these polydentate TSCN ligands was observed,

[a]*Advanced Porous Materials Unit (APMU), IMDEA Energy Institute, Av. Ramon de la Sagra 3, 28935 Móstoles-Madrid, Spain. E-mail: patricia.horcajada@imdea.org*
[b]*Department of Inorganic Chemistry Universidad Autonoma de Madrid, 28049 Madrid, Spain. E-mail: adoracion.gomez@uam.es*
[c]*Univ Pisa, Dept Chem & Ind Chem DCCI, Via Moruzzi 13, I-56124 Pisa, Italy. E-mail: tarita.biver@unipi.it*

†Electronic supplementary information (ESI) available. CCDC 2119429. For ESI and crystallographic data in CIF or other electronic format see DOI: https://doi.org/10.1039/d2qi02424a

‡Actual address: Environment and Agronomy Department, Instituto Nacional de Investigación y Tecnología Agraria y Alimentaria (INIA, CSIC).

demonstrating higher specificity in some of the palladium prototypes.[16] By changing the complex structure with diverse substituents in the TSCN structure, the cytotoxic profile could be modulated.

The mechanism of action of these promising metallodrugs implies the dissolution of the active species, remaining in contact with the components of the physiological media. Thus, the investigation of the compounds' active triggers ("activation process"), their stability ("aggregation, disruption effect or just integrity") and their pharmacological profile will provide meaningful data about specific interactions with the biological environment, such as their chemical equilibria and thermodynamics, commonly used to improve commercial product performance. In this sense, the thermodynamic process in solution has been deeply investigated, starting from the simplest aqueous media to more complex ones such as phosphate-buffered saline (PBS) and Tris-HCl/NaCl buffer or coordinating solvents such as DMSO (usually employed for *in vitro* assays). Although in most cases the solvent acts just as a simple spectator, in certain cases solvent coordination could trigger the inactivation of the metallodrug (*e.g.*, cisplatin).[17] It can also act as a transport solvent[18] or even impact their reactivity in aqueous media.[19]

Here, we present the synthesis and characterization of two novel palladium complexes derived from thiosemicarbazone ligands, modulating their reactivity in one of the prototypes by a particular DMSO coordination. Moreover, their complex stability in physiological media and therapeutic performance have been evaluated, revealing not only effective cytotoxicity against tumor cells but also, and more importantly, much lower toxicity to healthy cell lines. The study also embraces the analysis of the thermodynamic features of binding with nucleic acids and serum protein models.

2. Results and discussion

2.1. Synthesis and characterization of the palladium complexes

The synthesis of the palladium(II) complexes is depicted in Chart 1. The thiosemicarbazone ligand was not commercially available and was prepared by a condensation reaction following general procedures optimized in our laboratory (see the Experimental section for details).

2.1.1. Complex $[Pd(L)_2]$. Complex $[Pd(L)_2]$ was synthesized by the reaction of $Li_2[PdCl_4]$ with the ligand (LH) as described in the Experimental section.

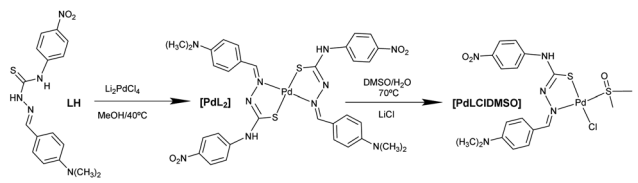

Chart 1 Synthesis pathway of the synthesized Pd(II) complexes.

Elemental analysis indicated a general formula of $[Pd(L)_2]$ and the mass spectra corroborated the formula with the molecular ion peak at 790.2 m/z $[Pd(L)_2]^+$ (see the Experimental section), whose isotopic distribution agrees with the proposed structure. Complex $[Pd(L)_2]$ was also characterized in solution by ^{1}H- and ^{13}C-NMR. The ^{1}H-NMR spectra showed a similar pattern as the ligand with the expected changes in the chemical shifts induced by the coordination of the metal. To assign all the signals accurately, the two-dimensional (2D) [^{1}H, ^{13}C] HMQC and HMBC NMR spectra were recorded. The aromatic part of the HMBC spectra is shown in Fig. S1.†

The most significant proton shift changes were observed at H2 and H8 from the phenyl groups (see the collected proton shift assignation in the Experimental section) and in the imine proton H6 as a direct consequence of the palladium coordination. This coordination also affects the corresponding C6 chemical shift at the ^{13}C-NMR spectra. In addition, the N–H group disappears, supporting ligand coordination in a thiolic form.

2.1.2. Complex [PdLCl(DMSO)]. The addition of a saturated aqueous LiCl solution to a DMSO solution of the $[Pd(L)_2]$ complex results in a ligand/solvent exchange reaction, in which one of the TSCN ligands is replaced by DMSO and a subsequent chloride anion coordination. After 3 days of reaction at 70 °C, a new neutral square planar complex of Pd(II), [PdLCl(DMSO)], was isolated and characterized by ^{1}H-NMR, ^{13}C-NMR and 2D [^{1}H, ^{13}C] HMQC and HMBC NMR. Fig. S2† shows the aliphatic area from the HMBC spectrum where the new signal from the coordinated DMSO is clear. No changes are observed in the aromatic part (Fig. S3†) compared to the spectra of the $[Pd(L)_2]$ complex shown in Fig. S1.†

In the IR spectrum of complex [PdLCl(DMSO)], the most indicative bands are the ν(S=O) vibrations corresponding to the coordinated DMSO, and the ν(Pd–Cl) band, whose values are comparable with other similar complexes found in the literature.[20]

The molecular structure of [PdLCl(DMSO)] was confirmed by single crystal X-ray diffraction (SC-XRD, Fig. 1A). The metal ion shows a square planar symmetry formed by the sulphur–

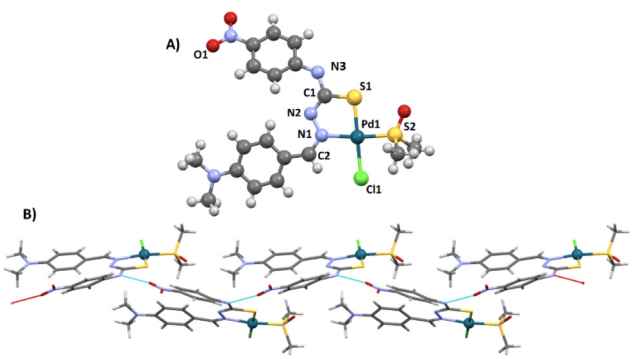

Fig. 1 (A) Molecular structure of [PdLCl(DMSO)], palladium in dark blue, sulphur in yellow, carbon in grey, oxygen in red, nitrogen in blue, hydrogen in light grey, chlorine in green. (B) Hydrogen bonding network within the crystal unit, contacts in cyan lines.

nitrogen donor atoms from the mono-deprotonated TSCN, and the sulphur atom from DMSO and a chlorine atom occupy the other two sites. The central palladium ion shows bond angles close to 90°, possibly caused by the lower steric hindrance produced by the chloride and DMSO ligands.

The found bond distances are comparable to other similar reported Pd(II)-TSCN complexes: Pd–N 2.076 Å (1.960–2.062), Pd–S_{TSCN} 2.234 Å, Pd–S_{DMSO} 2.249 Å (2.23–2.26) and Pd–Cl 2.349 Å (2.30). Although the Pd–N distance is slightly larger than the published range, it is shorter than the sum of the covalent radii.[20–22] The TSCN distances of the C–N and N–N bonds are between single and double bonding, in agreement with the tautomerization of TSCN to its thiolate form (acting as the monoanion), which results in the coordination to Pd (II).[23] In addition, the crystal structure shows an infinite network stabilized by the formation of hydrogen bonds *via* the N4–H and the O1 of adjacent complexes (achieving dimensions ~10.7 Å from the most peripheral moieties). This hydrogen bond is particularly strong since the three atoms (N4–H···O1) are aligned (180°; Fig. 1B). A table with selected distances and angles has been included in the ESI (Table S1†).

2.1.3. Conversion of $[Pd(L)_2]$ in solution to [PdLCl(DMSO)]. The monitoring study of the stability of complex $[Pd(L)_2]$ in DMSO solution by NMR showed no changes after 24 h (Fig. 2A).

The addition of D_2O/H_2O to the sample produced a very small interchange with the acidic protons (Fig. 2B and C). The sample was also stable using D_2O saturated with NaCl for 3 days, with no signals of coordinated DMSO coming up in the NMR spectra (Fig. 2D and E). However, DMSO coordination emerged using LiCl after 3 days, with a small new signal arising at 2.55 ppm (Fig. 2F). The process is extremely slow: only after 3 days and increasing the temperature at 70 °C the DMSO coordination complex becomes the major product. The signal corresponding to the coordinated DMSO appears slightly deshielded compared to the free solvent (Fig. 2F, asterisk), which is a clear indication of solvent coordination.

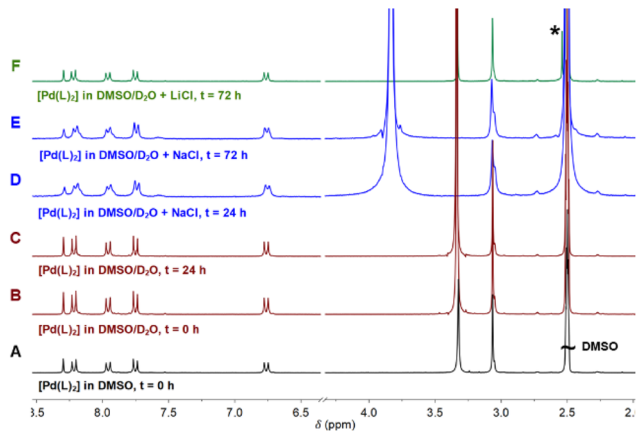

Fig. 2 ^{1}H-NMR spectra of complex $[Pd(L)_2]$ (A) in DMSO-d_6, (B) DMSO-d_6 and D_2O t = 0, (C) DMSO-d_6 and D_2O t = 24 h, (D) DMSO-d_6 and D_2O/H_2O saturated with NaCl at t = 24 h, (E) DMSO-d_6 and D_2O/H_2O with saturated NaCl at t = 72 h, or (F) DMSO-d_6 and D_2O with saturated LiCl at t = 72 h.

This palladium complex reactivity toward DMSO is consistent with some platinum complexes reported in the literature, where the addition of water triggered the coordination.[19]

However, to the best of our knowledge, this is the first time that such behaviour is reported for palladium complexes, though such a coordination is not as quick as that observed for platinum and needs higher temperatures, longer times, and excess stabilizing counterions. Moreover, we have here accomplished the required conditions to isolate both forms and compared them. The conversion at the scaled reaction only took place in the presence of LiCl and not with NaCl. At the scaled amounts used in the reaction (see the Experimental section), the quantity of DMSO is higher and LiCl becomes a better source of chloride anions because of its higher covalency and solubility in organic solvents. On the other hand, common salts, such as NaCl (buffer present in physiological solution), are more effective in diluted solutions such as those used in UV and biological experiments.

2.2. Stability of $[Pd(L)_2]$ and [PdLCl(DMSO)] complexes in buffered solutions

Once the reactivity of the complexes was determined under the synthetic conditions, we further investigated their stability under more complex media closer to physiological ones, such as aqueous solutions and different complex buffers. In this sense, we first monitored the stability of Pd complexes in water (containing 3 or 5% DMSO) from fresh up to 24 h contact times by UV-Vis spectroscopy (Fig. S4A†), highlighting the lack of significant changes during the first 24 h for [PdLCl(DMSO)]. This is also in agreement with the hydrodynamic particle size, determined by dynamic light scattering (DLS): an average size of 15 ± 4 and 16 ± 3 nm with a positive surface charge of +27 ± 6 and +42 ± 8 mV were maintained up to 24 h for $[Pd(L)_2]$ and [PdLCl(DMSO)], respectively. However, after a 24 h contact time, $[Pd(L)_2]$ showed a gradual concentration decrease. This effect could be explained by the formation of aggregates (reported previously in TSCN complexes),[24] or by the complex disruption due to the impact of other physiological parameters (*e.g.*, pH, secondary reactions), which could lead to the formation of less soluble complexes. Here, the decrease in the particle size has been associated with the absence of aggregation after 24 h in water, supporting the complex disruption hypothesis.

We also investigated the stability of compounds by adding NaCl (4μM) which is a known electrolyte existing in biological media. The spectral profile (Fig. S4B†) did not show significant changes in comparison to the Tris-HCl aqueous solution (Fig. S4A†).

To further investigate the stability of $[Pd(L)_2]$ and [PdLCl(DMSO)], their UV-Vis profiles were monitored by varying the concentration at 37 °C in Tris-HCl solutions as a common buffer used to study potential DNA interactions (Fig. S5A and B†). The findings showed that the Lambert–Beer law is obeyed in the 0–60 μM concentration range (Fig. S5C†). This behav-

iour suggests the absence of complex–complex interactions, also confirmed by the consistency of absorbance ratios at two different wavelengths: 299/371 nm and 300/371 nm for $[Pd(L)_2]$ and [PdLCl(DMSO)], respectively (Fig. S5D†). The molar extinction coefficient (ε) values calculated from this experiment are (at the wavelengths of maximum, 371 nm in both cases) 1.11×10^4 M^{-1} cm^{-1} for $[Pd(L)_2]$ and 1.05×10^4 M^{-1} cm^{-1} for [PdLCl(DMSO)].

For a better understanding of the target complexes and to mimic specific biological scenarios (*e.g.* serum, intravenous administration), the stability of both complexes was studied not only in simple aqueous solution but also in more complex conditions, including phosphate-buffered saline (PBS) and Tris-HCl/NaCl buffers under different temperatures (25–95 °C). The thermodynamics of the complex species in solution was checked by monitoring their UV-Vis spectra (Fig. S6†). The absorption profile of $[Pd(L)_2]$ complex showed a steeper concentration decrease in comparison with the [PdLCl(DMSO)] profile, being higher in Tris-HCl/NaCl compared to PBS. This change could be related to a potential degradation in the presence of Tris-HCl since NaCl concentration is lower (150 *vs.* 100 mM for PBS/Tris-HCl, respectively). As discussed before, no conversions were observed in the presence of NaCl at the concentrations used in the NMR stability experiment (see section 2.1.3.) because of the higher concentration of DMSO. This conversion was only detected with LiCl which is a better chloride donor in the mixture of solvents used in the reactivity study. Moreover, both complexes displayed suitable thermal stability up to 37 °C.

2.3. Cytotoxic activity

One of the requirements of effective chemotherapeutics is the large *in vitro* and/or *in vivo* growth-inhibitory capability associated with fewer side effects. Before investigating their therapeutic performance through an MTT toxicological assay (see the Experimental section and Fig. 3, where they had been compared with each precursor effect and a recognized reference drug, cisplatin), their stability in cell culture media was also evaluated. A nanoscale particle size was observed in both complexes, displaying a slight increase after 72 h (6 ± 2 nm at $t = 0$ in both cases to 55 ± 22 and 38 ± 12 nm at $t = 72$ h for $[Pd(L)_2]$ and [PdLCl(DMSO)], respectively). This average size is in agreement with the nanometric values obtained in a simpler medium such as an aqueous solution. However, the presence of biological components in the cell culture media (proteins, salts, electrolytes, serum, *etc.*) favors their attachment on the external surface of the complexes, resulting in a larger size and the inversion of their ζ-potential (from cationic values, +27 ± 6 and +42 ± 8 mV to a slightly negative surface, −9 ± 1 and −8 ± 1 mV for $[Pd(L)_2]$ and [PdLCl(DMSO)], respectively). Once the complex stability was confirmed, the cytotoxicity was evaluated. For this purpose, two different human cancer cells were selected: (i) PC-3 cells ("prostate cancer"), the most diagnosed cancer in males and the 2nd highest cause of male cancer-related deaths[25] and (ii) colon adenocarcinoma Caco-2 cells ("colorectal cancer"), the 3rd most frequent type of cancer and

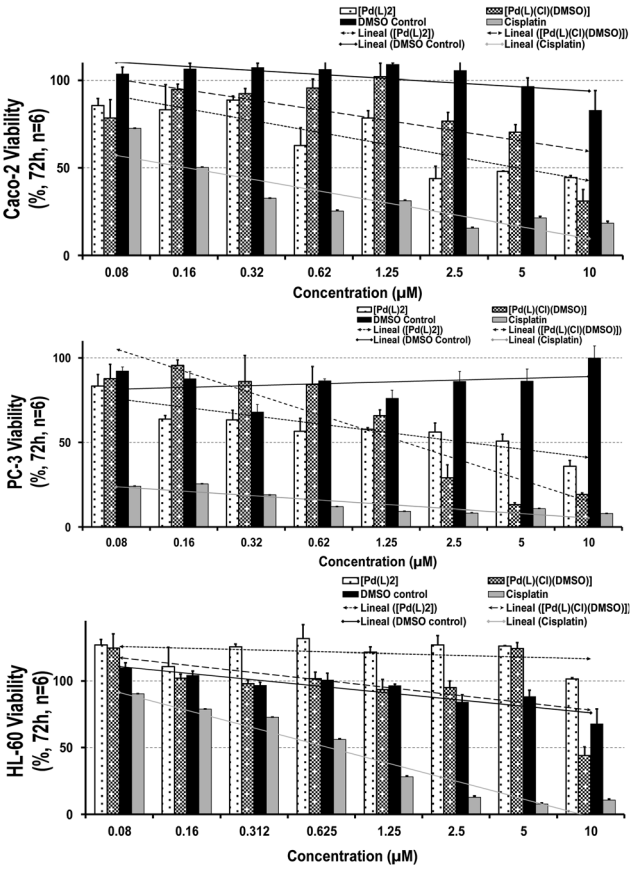

Fig. 3 Cell viability and tendency line of (A) Caco-2, (B) PC-3 and (C) HL-60 cell lines after 72 h incubation with $[Pd(L)_2]$ (white dots), [PdLCl(DMSO)] (grey dots) complexes, the DMSO control (black) and cisplatin (grey). Note that the shown data corresponds to the average of triplicate for each concentration, obtained in two independent experiments (a total of $n = 6$). The vertical error bars drawn in the diagram indicate the range of fluctuations from which the standard deviations were calculated. Note the absence of cytotoxicity of the $K_2[PdCl_4]$ precursor, highlighting the role of the whole Pd-complex.

well-characterized intestinal barrier model, extensively used over the past few years for preclinical studies of diverse therapeutic agents.[26,27] Moreover, a promyelocytic HL-60 cell line was also chosen to evaluate the selectivity against healthy cells. In addition, this immunological cell line, able to proliferate/differentiate to myelomonocytic lineage (granulocytes, monocytes, macrophage and eosinophils),[28–30] is involved in relevant biological processes, including the cellular redox homeostasis (ROS) and immune system activation.

Remarkably, after 72 h-contact, both palladium complexes were able to decrease the cell-growth capability in tumor cells (being slightly higher for $[Pd(L)_2]$ in comparison with the DMSO control), exhibiting a stronger cytotoxic profile on prostatic than the gastrointestinal cell line. The IC_{50} values (50% maximum inhibitory concentration) reached a dose of 2.50 and 1.25 μM for Caco-2 and PC-3 cells, respectively, which suggests elevated responsiveness by prostatic cells (Fig. 3; Table S2†). In contrast, both complexes did not show particu-

lar toxicity to the myelomonocytic HL-60 cells (IC_{50} values ≥10 μM), displaying similar selectivity index values (~0.09–0.026) than our reference compound, cisplatin. When comparing these outcomes, a higher toxicity profile was observed than that obtained by cisplatin, not only against tumor but also against healthy immune cells (even at the lowest concentration: IC_{50} values ~0.16 μM in Caco-2, <0.08 μM in PC-3 and 0.62 μM in HL-60 for cisplatin), showing severe and invasive actions. Thus, their moderate antitumoral effect and similar selectivity index against cancer lines together with a gentler healthy performance of both palladium complexes make them promising chemotherapeutic agents.

To better understand the specific growth-inhibitory capability of the palladium complexes against tumor cells, their impact on the cell cycle of each cell line was investigated by flow cytometry. The general trend is the activation of cell checkpoints, arresting the cycle progression and attempting to repair the cellular damage. This process generally contributes to the growth inhibition effect (no cell death needed), resulting in the higher presence of mitotic catastrophes before entering into apoptosis (typically premature stage in S phase-arrested cells or after bypassing the G2 arrest).[31–33] After 72 h of contact time, the majority of the cell population was arrested in an S-phase (~88%, see Table S3†), with no substantial difference. This strong accumulation in the S-phase could be associated with the increase of mitotic processes, and consequently, to greater entrance into apoptosis. However, more specific molecular or gene expression analyses (*e.g.* caspase 3/7 enzyme assay, Cyclin A-Cdk2 activity, *etc.*) need to be performed to better understand the processes involved in their mechanism.

Overall, both palladium complexes are promising chemotherapeutic agents because of their antitumoral effect, similar selectivity index against cancer lines and their gentler healthy performance.

2.4. Cellular uptake

Some palladium derivatives are able to intercalate the DNA strands, blocking cellular replication. However, there are also other potential molecular mechanisms (*e.g.*, induction of apoptosis, necrosis) that can trigger DNA damage and, consequently, tumor cell death. One of the main factors involved in successful chemotherapy is the cellular internalization of these compounds to provide the safest and most effective therapeutic dose.[34] In this sense, cellular uptake was investigated in the selected tumor cell lines in order to evaluate not only the cell internalization (cytoplasmic content) but also the specific nuclear location of both complexes. For these purposes, 5 μM complexes and their respective precursors were incubated with cells for 72 h, isolating both the cytoplasmic and nuclear fractions for metal quantification by ICP-MS (more details in the Experimental section). Remarkably, all treatments were able to cross the cell membrane, reaching the cytoplasm and nuclear compartment in both cell lines, being slightly boosted for the tumor gastrointestinal cells (Caco-2; Table 1 and Fig. S7A†). Regarding the performance of complexes, $[Pd(L)_2]$ showed a larger cellular amount, mainly in the nucleus (1/0.2% *vs.* 12/3% for the Caco-2 and PC-3 cytoplasm/nucleus, respectively). Furthermore, the cellular uptake and nucleus targeting of the [PdLCl(DMSO)] complex were higher than those of $[Pd(L)_2]$, regardless of the cell line (0.7/0.3% *vs.* 0.2/1% for the Caco-2 and PC-3 cytoplasm/nucleus, respectively). Compared with the cisplatin reference, lower levels of both complexes were detected in the cytoplasm and nucleus, reaching approximately 3- and 39-times lower concentrations than cisplatin in Caco-2 and PC-3, respectively. This agrees with the previously observed reduced cytotoxic profile of the Pd-complexes when compared with cisplatin.

Table 1 Metal content (μg L^{-1}) and cellular uptake (%) extracted from the nucleus (N) and the cytoplasm (C) of Caco-2 and PC-3 cells after cell internalization (72 h) of $[Pd(L)_2]$, [PdLCl(DMSO)] and cisplatin

Metal content (μg L^{-1}) -				
Cell uptake[a] (%)				
	Caco-2		PC-3	
Complex	N	C	N	C
$[Pd(L)_2]$	78.60 *(12%)*	7.78 *(1.2%)*	19.11 *(2.8%)*	1.64 *(0.2%)*
[PdLCl(DMSO)]	1.67 *(0.2%)*	6.89 *(0.7%)*	9.70 *(1.0%)*	2.78 *(0.3%)*
Cisplatin	$<1.10^3$ *(24.1%)*	$>6.10^3$ (>99%)	$>1.10^3$ *(38.4%)*	$<1.10^2$ *(2.4%)*
Control -	2.78 *(0.3%)*		2.78 *(0.3%)*	
$K_2[PdCl_4]$	2.78 *(0.3%)*	0.41 *(0.0%)*	2.78 *(0.3%)*	

[a] Estimated according to the molecular weight and metal abundance in each compound.

2.5. Interaction with biological targets

2.5.1. DNA binding. Given that cellular effects were evidenced and the known relationship between possible antitumoral activity and the binding to nucleic acids, we studied the possible interactions of the complexes with the genetic material. We performed UV-Vis titrations at 25 °C with natural calf thymus DNA (CT-DNA). The titrant (CT-DNA) addition to the metal complex solution, after dilution effects are corrected, still produces signal changes that confirm that a binding does indeed take place (Fig. S8A and B†). The binding isotherms can be constructed by plotting the absorbance values as the signal change $(A - \varepsilon_{complex}C_{complex})/C_{complex}$ at a fixed wavelength *vs.* the added polynucleotide concentration (Fig. 4). Both compounds possess a strong affinity to CT-DNA, as observed by the sharp curvature of the corresponding binding isotherms (Fig. 4, open circles). The binding constant values (Table 2, see paragraph 2.5.2 for data analysis details) are in line with the literature data on other Pd(II)-thiosemicarbazone/DNA systems (Table S4†), placing at the upper limit of the log *K* range.

2.5.2. RNA binding and comparison with DNA. The spectrophotometric titrations were also repeated with synthetic RNA polynucleotides in the single (poly(rA)), double

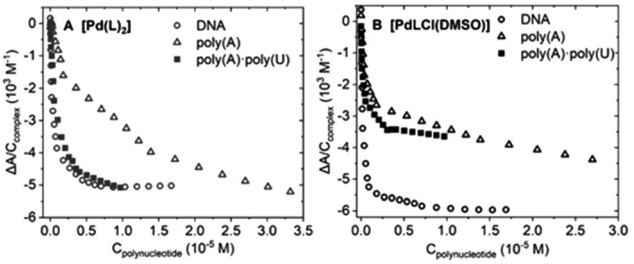

Fig. 4 Binding isotherms of the spectrophotometric titrations of complexes (A) $[Pd(L)_2]$ and (B) [PdLCl(DMSO)] constructed with the absorbance data at 371 nm. $C_{complex}$ = 1.06 × 10^{-5} M, Tris-HCl 5 mM, NaCl 100 mM, pH 7.4, 25.0 °C.

Table 2 Binding constants (log K ± standard deviation) obtained from the spectrophotometric (for BSA spectrofluorometric) titrations for the interaction between $[Pd(L)_2]$ and [PdLCl(DMSO)] and the quoted biomolecules. Tris-HCl 5 mM, NaCl 100 mM, pH 7.4, 25.0 °C for all the assays

	Log K			
Complex	DNA	PolyAU	PolyA	BSA
$[Pd(L)_2]$	6.0 ± 0.2	5.5 ± 0.3	5.4 ± 0.1	7.2 ± 0.1
[PdLCl(DMSO)]	6.1 ± 0.2	5.4 ± 0.3	5.1 ± 0.3	6.5 ± 0.1

(poly(rA)·poly(rU)) and triple (poly(rU)*poly(rA)·poly(rU)) strand forms (Fig. S8C–H†). The affinity to the double-stranded RNA is generally similar to that for DNA (Fig. 4, full squares), whereas the complexes show less affinity to single-stranded RNA (Fig. 4, open triangles). Note that, as for the affinity, we refer to the curvature of the plots and the tendency to reach saturation (plateau). On the other hand, the different amplitudes of the binding isotherms will be related to the different photophysical properties of the metal complex/polynucleotide adduct formed. The quantitative evaluation of the binding constant is better done by using the whole spectral range and not a single wavelength. Accordingly, based on the titration spectra, the HypSpec2014® software (HyperQuad, Leeds, UK) was used to quantify the complex binding to the different biosubstrates. Data analysis suggests that a 1 : 1 model (metal complex : base pair) is sufficient to describe the experimental behavior. The different binding constants are listed in Table 2.

Note that titrations with the triple-stranded RNA model poly(rU)*poly(rA)·poly(rU) were also carried out. RNA triplexes deserve high attention for many different reasons,[35] ranging from telomerase function[36] to viruses' self-protection mechanisms[37] and riboswitches regulating gene expression.[38] However, for both palladium complexes, no significant spectral change was recorded, which indicates the lack of interaction (Fig. S8G and H†). Nevertheless, this behavior may entail that both complexes interact with double-stranded polynucleotides *via* groove binding. In fact, in poly(rU)·poly(rA)·poly(rU), one of the grooves is occupied by the third strand, hampering the interaction between the complex and the nucleic acid.[39]

To confirm the groove binding mode, ethidium bromide (EtBr) displacement tests were undertaken. EtBr is a well-known DNA intercalator reported in many procedures.[40–42] Given the very different fluorescence emission of EtBr either as intercalated species or as a free probe, exchange tests are a recognized diagnostic tool to determine the polynucleotide affinity and penetration degree of non-fluorescent DNA-binding molecules.[43] In the fluorescence exchange titrations with EtBr, known amounts of each complex were directly added to EtBr-saturated CT-DNA and dsRNA, a potential fluorescence reduction at the characteristic excitation (ex)/emission (em) wavelengths of the DNA-EtBr or RNA-EtBr adduct would imply the EtBr displacement from the double helix, and therefore, the intercalation of the complexes into the DNA and/or the dsRNA strand. However, in both cases the fluorescence remains constant regardless of the complex addition (Fig. S9†), ruling out intercalation in favor of external/groove binding.

2.5.3. DNA plasmid model binding. Gel electrophoresis assays with bacterial DNA plasmid (pBR322) as a DNA model were performed to discard covalent interaction with nucleic acids. The electrophoretic mobility of the supercoiled plasmid pBR322 was investigated in the presence of the complexes, using the cisplatin covalent binder as a recognized control. Supercoiled pBR322 plasmid DNA is an extensively used model for evaluating the interaction of platinum compounds with a secondary structure DNA model.[44–46] It is very well-known that cisplatin can change the mobility of the pBR322 isoforms, slowing down the closed circular (SC) form (unwinding produced by the covalent interaction; see lane 11, Fig. 5) and increasing the mobility of the open circular (OC) form ("platination reaction") until both co-migrate (see lane 13, Fig. 5).[47] Non-covalent interaction is measured using the pure SC plasmid form.[43] Complexes $[Pd(L)_2]$ (lanes 3 to 6, Fig. 5) and [PdLCl(DMSO)] (lanes 7 to 10, Fig. 5) produce a slight unwinding of the SC conformation which does not agree with the significant degree of unwinding expected for the intercalation.[43] More importantly, the compounds did not alter the electrophoretic mobility of the OC isoform, which also implies a non-covalent DNA interaction.

Furthermore, to support the minor unwinding produced by the complexes, we have used an additional direct hydrodynamic technique (viscosity).

2.5.4. Viscosity. Viscosity is a direct parameter for studying drug–DNA interactions as a function of the hydrodynamic

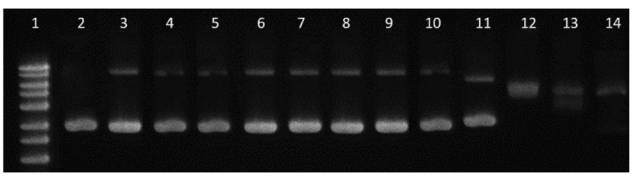

Fig. 5 Gel electrophoresis. Lane 1: 1 kb DNA ladder; lane 2: pBR322 control; lanes 3–6: $[Pd(L)_2]$ at r_i: 0.01 to 0.2; lanes 7–10: [PdLCl(DMSO)] at r_i: 0.01 to 0.2; lanes 11–14: cisplatin at r_i: 0.01 to 0.2. C_{DNA} = 0.0625 μg μL^{-1}.

changes induced by a binding agent. Changes in the DNA chain length produced by metallodrug binding can be distinguished from covalent to non-covalent since these binding modes display different hydrodynamic characteristics. The relative viscosity (η/η_0) is directly proportional to the cube of the contour length of the DNA: $\eta/\eta_0 = (L/L_0)^3$. For example, the presence of an intercalating molecule (such as ethidium bromide) increases the dynamic viscosity of the solution containing the DNA. The intercalative mode increases the separation of the base pairs and therefore lengthens the DNA double helix.[48]

By contrast, groove binders such as Hoechst DNA 33258 fluorescent dye do not alter the length of the DNA significantly, causing minimal changes to the viscosity of the solution. In the case of a covalent binder such as cisplatin, the relative viscosity of the solution decreases.[43]

Fig. 6 shows the variation in the viscosity of CT-DNA solution upon the addition of the complexes [PdL_2] and [Pd(L)Cl (DMSO)]. Cisplatin and ethidium bromide (EtBr) are also added to the experiment.

The results obtained for cisplatin and EtBr are in agreement with the data reported in the literature for a covalent binder and an intercalator, respectively. The relative viscosity of CT-DNA remains certainly unchanged upon the addition of both palladium compounds. There are not very significant variations in the viscosity, and this is more in agreement with the viscosity profile of typical DNA groove binders instead of intercalators or covalent binders.

Both complexes show a very similar profile in which electrostatic interplay is discarded as both complexes are neutral. Thus, considering all the above-mentioned results, groove binding is confirmed to be the most plausible mechanism of interaction.[49]

2.5.5. BSA binding. Following the biological examination, protein binding to the complexes was assessed to simulate a real serological scenario upon intravenous administration. Bovine serum albumin (BSA) was selected as it is one of the most common proteins found in the bloodstream. The titrations were performed both spectrophotometrically and spectrofluorimetrically. However, the absorbance titrations of [$Pd(L)_2$] and [PdLCl(DMSO)] with BSA were discarded as non-conclusive (non-significant signal changes). Fig. 7A and B show the changes in the BSA fluorescence emission upon the addition of increasing amounts of [$Pd(L)_2$] and [PdLCl (DMSO)], respectively. The fluorescence emission spectrum undergoes a signal shift and decreases in the case of both [$Pd(L)_2$] and [PdLCl(DMSO)], reflecting an interaction at work. Eqn (1) was applied to titration data in order to find out the binding stoichiometry (n) of the complex to BSA and the binding constant (K') of the metal complex to BSA (Fig. 7C).

Equation applied to the titration data:

$$\frac{C_{BSA}(C_M\Delta\varphi - \Delta F)}{\Delta F} = \frac{1}{nK'} + \frac{(C_M\Delta\varphi - \Delta F)}{\Delta\varphi}\frac{1}{n} \quad (1)$$

The binding constant could not be evaluated by eqn (1) due to an intercept too close to zero ($K' > 10^6$): this finding confirms the very high affinity for the biosubstrate and the formation of a metal complex/BSA adduct (the quenching effect is not due to collisional quenching only).[50] The same analysis indicates that a binding stoichiometry of $n = 1.1 \pm 0.1$ holds for both systems. The confirmation of 1 : 1 binding allows the evaluation of K' using the HypSpec2014® software, which considers all the wavelengths of the fluorescence titration spectra.

The binding constants for [$Pd(L)_2$]/BSA and [PdLCl(DMSO)]/BSA interaction are listed in Table 2. The calculated constants are in line with the window for exogenous drug transportation: the binding is strong enough to actually form an adduct but,

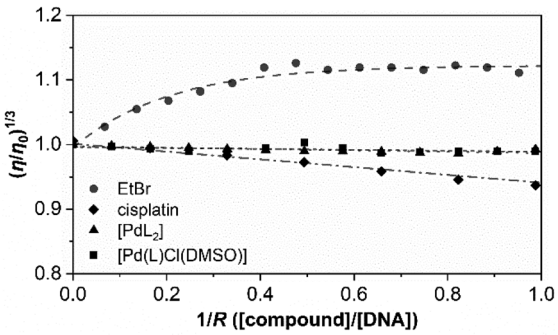

Fig. 6 Effect of increasing amounts of complexes [PdL_2] (triangles) and [Pd(L)Cl(DMSO)] (squares) on the viscosity of CT-DNA. Cisplatin and ethidium bromide (EtBr) are included as a reference (rhombi and circles, respectively). The data were collected for [DNA] = 5.69×10^{-5} M and different 1/R ratios (R = [DNA]/[compound], from 0.0 to 1.0). Tris-HCl 5 mM, NaCl 100 mM, pH 7.35, 25.0 ± 0.1 °C.

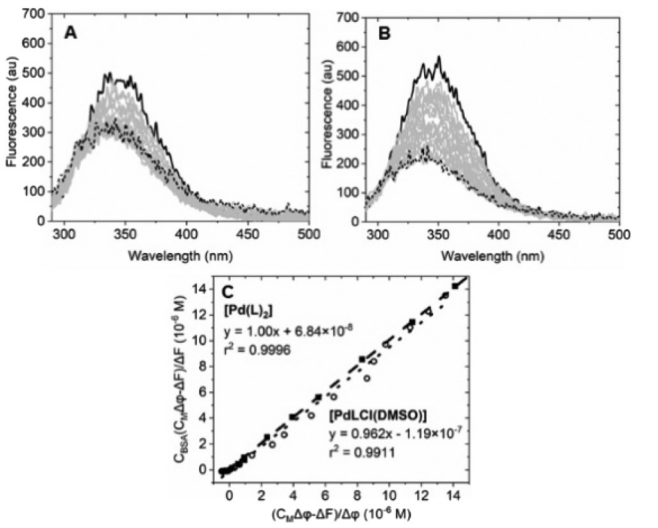

Fig. 7 Spectrofluorimetric titration of (A) [$Pd(L)_2$]/BSA ($C_{complex}$ from 0 (solid) to 2.75×10^{-5} M (dotted), $C_{BSA} = 6.22 \times 10^{-7}$ M); (B) spectrofluorimetric titration of [PdLCl(DMSO)]/BSA ($C_{complex}$ from 0 (solid) to 1.41×10^{-5} M (dotted), $C_{BSA} = 6.22 \times 10^{-7}$ M). (C) Plot of eqn (1) at λ = 345 nm for the [$Pd(L)_2$]/BSA (full squares) and the [PdLCl(DMSO)]/BSA (open circles) titrations. λ_{exc} = 280 nm, λ_{em} = 345 nm. Tris-HCl 5 mM, NaCl 100 mM, pH 7.4, 25 °C.

at the same time, weak enough so that the drug can be released once it gets to the target.[51,52]

3. Conclusion

We report on the synthesis of two novel palladium–thiosemicarbazone complexes and their speciation in solution, demonstrating their stability in buffers and clarifying the role of coordinating solvents such as DMSO. Both species strongly interact with DNA/RNA models, where the absence of interaction with the triple-stranded RNA indicates a groove binding mode. Moreover, the binding constant with serum albumin is within the transportation window. We obtained interesting results as both drugs are not only efficient in selected tumor cells from the most common human cancer disease, but more specific than cisplatin *versus* non-cancer cells.

4. Experimental

4.1. Materials

The chemicals were purchased from Johnson and Matthey, Sigma-Aldrich and VWR. pBR322 was purchased from Fisher Scientific and Calf thymus DNA (CT-DNA), as lyophilized sodium salt, from Sigma-Aldrich. The stock solutions were prepared by dissolving known amounts in ultrapure water and were standardized spectrophotometrically (ε = 13 200 M^{-1} cm^{-1} at 260 nm). Polyriboadenylic (poly(rA)), polyriboadenylic·polyribouridylic (poly(rA)·poly(rU)) and polyuridylic (poly (rU)) acids were purchased from Sigma as their potassium salts. The stock solutions (in water) were standardized spectrophotometrically (ε = 14 900 M^{-1} cm^{-1} at 260 nm for poly (rA)·poly(rU) and ε = 8900 M^{-1} cm^{-1} at 260 nm for poly (rA)·poly(rU)). Poly(rU)·poly(rA)·poly(rU) was obtained at pH 7.0 by the quantitative reaction between equimolar amounts of poly(rU) and poly(rA)·poly(rU). Ethidium bromide was purchased from Sigma. Its stock solution was prepared by dissolving suitable amounts of the solid in water and was standardized spectrophotometrically (ε = 5700 M^{-1} cm^{-1} at 480 nm).

4.2. Methods

NMR spectra were recorded, at room temperature, using a two-channel 300 MHz Bruker Avance III-HD Nanobay spectrometer equipped with a 5 mm BBO 1H/X probe and *Z* gradients, located at SIdI. SIdI stands for Interdepartmental Investigation Service. DMSO-d_6 was used as the solvent (containing 0.05 vol% tetramethylsilane (TMS) as a reference). Chemical shift values are given in ppm relative to the residual TMS signals. The following abbreviations were used: s (singlet), d (doublet) and m (multiplet). Elemental analyses were performed on a LECO CHNS-932 elemental analyzer located at SIdI. Analyses of the mass spectra were performed using FAB^+ (fast atom bombardment) in a Waters VG AutoSpec mass spectrometry unit using MALDI (matrix-assisted laser desorption/ionization) with a Bruker Ultraflex III (MALDI-TOF/TOF) mass spectrometry unit, both located at SIdI. Infrared (IR) spectra were recorded using a PerkinElmer Model 283 spectrometer with an attenuated total reflectance (ATR) MIRacle Single Reflection Horizontal accessory and equipped with CsI optical windows for spectra between 600 and 200 cm^{-1} in Nujol mull preparations. Absorbance spectra were recorded using a Shimadzu UV-2450 double-beam UV-Vis spectrophotometer (Kyoto, Japan), whereas fluorescence spectra were recorded with an LS55 PerkinElmer spectrofluorometer (Waltham, MA, USA). Both instruments were equipped with temperature control within ±0.1 °C. For particle size and ζ-potential determinations, each complex was diluted from the DMSO stock (5 mM) with the desired media (aqueous solution, cell culture media – see Table 3: supplemented DMEM (Dulbecco's modified Eagle's medium) & RPMI (Roswell Park Memorial Institute Medium), being analyzed with a Malvern Nano-ZS, Zetasizer Nano series. Once the suspensions were prepared, an ultrasonication step followed (ultrasound tip at 10% amplitude for 1 min), monitoring the particle size evolution from t = 0 to 24 h.

4.3. Synthesis of the compounds

4.3.1. Ligand. The ligand synthesis required *p*-nitrophenylthiosemicarbazide as starting material which is not commercially available. We prepared it following a reported procedure with slight changes in the purification procedure.[33] Briefly *p*-nitrophenylthiosemicarbazide was prepared as follows. To a suspension of *p*-nitrophenyl isothiocyanate (1.0043 g, 5.57 mmol) in acetonitrile (20 mL) cooled in an ice bath, a solution of hydrazine hydrate (0.54 μL, 11.1 mmol) in acetonitrile (15 mL) was added dropwise and the reaction was maintained with constant stirring for 1 hour, obtaining a brown solid that was filtered, washed with acetonitrile and vacuum dried. The product was purified by chromatography in silica gel, using CH_2Cl_2 and CH_2Cl_2 : EtOH 99 : 1 as eluents. The final product was eluted last and concentrated to dryness, isolating 712.6 mg of a yellow solid. Yield: 60%. FAB^+-MS (*m*/*z*): $[M + CH_3CN]^+$: 253. ^{1}H-RMN (300 MHz, DMSO-d_6), δ (ppm): 8.07 (d, 2H, H6); 8.21 (d, 2H, H7); 10.26 (s, 1H, N–H2); 10.76 (s, 1H, N–H4). ^{13}C-RMN (DMSO-d_6), δ (ppm): 123.45, 123.70, 143.06, 145.45, 175.74. IR (cm^{-1}): ν_a (NH_2): 3336; ν_s (NH_2): 3241; ν (NH): 3211; δ (NH_2): 1637; ν_a (NO_2): 1506; ν_s (NO_2): 1334; ν (C=S): 848.

HL: *N*1-(4-(dimethylamino)benzylidene)-*N*4-(4-nitrophenyl) thiosemicarbazone: an ethanolic solution (1.5 mL) of *p*-dimethylaminobenzaldehyde (11.3 mg, 0.076 mmol) was added dropwise to a solution of *p*-nitrophenylthiosemicarbazide (16.1 mg, 0.076 mmol) in AcOH 6% (2 mL) at 50 °C. The mixture was stirred and heated to the reflux temperature for 5 hours. An orange solid was isolated after cooling by filtration and washed several times with very cold portions (5 mL) of ethanol and cold methanol. Finally, the solid was recrystallized into CH_2Cl_2, filtered and vacuum dried. Yield: 66%. Orange solid. Elemental analysis (%) for $C_{16}H_{17}N_5O_2S{\cdot}H_2O$: calculated: C, 53.17; H, 5.30; N, 19.38. Experimental: C, 52.81; H, 4.91; N, 19.27. FAB^+-MS (*m*/*z*): $[M]^+$: 343.2; $[M + H]^+$: 344.2. ^{1}H-RMN

Table 3 Media composition (g L^{-1}; pH: 7.2) based on amino acids, inorganic salts and vitamins, suitable for cell culture applications

Components			Components		
Amino acids	DMEM	RPMI	Vitamins	DMEM	RPMI
Glycine	0.40	0.01	Choline chloride	0.004	0.003
L-Alanyl-glutamine	—	—	D-Calcium pantothenate	0.004	0.00025
L-Arginine hydrochloride	0.08	—	Folic acid	0.004	0.001
L-Cystine	0.06	0.06	Niacinamide	0.004	0.001
L-Histidine hydrochloride	0.04	0.015	Pyridoxal hydrochloride	0.004	0.001
L-Isoleucine	0.10	0.05	Riboflavin	0.0004	0.0002
L-Leucine	0.10	—	Thiamine hydrochloride	0.004	0.001
L-Lysine hydrochloride	0.15	—	i-Inositol	0.007	—
L-Methionine	0.03	0.015	**Inorganic salts**		
L-Phenylalanine	0.07	0.015	Calcium chloride	0.30	0.10
L-Serine	0.04	0.03	Ferric nitrate	0.0001	—
L-Threonine	0.90	0.02	Magnesium sulfate	0.10	0.05
L-Tryptophan	0.02	0.005	Potassium chloride	0.40	0.40
L-Tyrosine disodium salt dihydrate	0.12	0.03	Sodium bicarbonate	3.7	2.00
L-Valine	0.09	0.02	Sodium chloride	6.40	6.00
Amino acids	**DMEM**	**RPMI**	Sodium phosphate monobasic	0.11	0.80
Glycine	0.40	0.01			
Others	**DMEM**	**RPMI**	**Others**	**DMEM**	**RPMI**
D-Glucose	25.00	4.50	Penicillin–streptomycin	1.00	
Phenol red	0.04	0.01	MEM non-essential amino–acid solution	1.00	
Fetal bovine serum	10.00				

(300 MHz, DMSO-d_6), δ (ppm): 2.98 (s, 6H, H11); 6.74 (d, 2H, H9); 7.70 (d, 2H, H8); 8.10 (d, 3H, H2 and H6); 8.23 (d, 2H, H3); 10.29 (s, 1H, N–HA); 11.96 (s, 1H, N–HB). ^{13}C-RMN (DMSO-d_6), δ (ppm): 39.52 (C11), 111.59 (C9), 120.70 (C7), 123.59 (C2), 123.64 (C3), 129.31 (C8), 143.13 (C1), 145.25 (C6), 145.62 (C4), 151.75 (C10), 174.03 (C5). IR (cm^{-1}): ν (NH): 3254, 3118; ν (C=N): 1611; ν_a (NO_2): 1501; ν_s (NO_2): 1330; ν (C=S): 843.

4.3.2. Complex [Pd(L)$_2$]. $Li_2[PdCl_4]$ was prepared *in situ* following the reported methodology.[53] Briefly, $PdCl_2$ (62.70 mg, 0.354 mmol) was mixed with LiCl (61.37 mg, 1.45 mmol) in methanol (10 mL), under an inert atmosphere. The mixture was kept under constant stirring at 40 °C for 15 minutes, and then a solution of the LH ligand (121.27 mg) was added dropwise (0.353 mmol) to methanol (20 mL). The reaction mixture was maintained under an inert atmosphere and temperature was raised to 65 °C for 9 days. The dark burgundy solid obtained was filtered, washed with water and methanol and vacuum dried. The solid was cracked with hexane for further purification, filtered and vacuum dried to obtain 93.03 mg of the product.

[Pd(L)$_2$]. Dark burgundy colour. Yield: 54%. Elemental analysis (wt%) for $C_{32}H_{32}N_{10}O_4S_2Pd{\cdot}3H_2O$: calculated: C, 48.58; H, 4.08; N, 17.70. Experimental: C, 48.13; H, 3.88; N, 17.34. MALDI-MS (*m*/*z*): $[M]^+$: 790.2. ^{1}H-RMN (300 MHz, DMSO-d_6), δ (ppm): 3.07 (s, 6H, H11); 6.76 (d, 2H, H9); 7.75 (d, 2H, H2); 7.96 (d, 2H, H8); 8.22 (d, 2H, H3/3′); 8.30 (s, 1H, H6); 10.30 (s, 1H, N–HA). ^{13}C-RMN (DMSO-d_6), δ (ppm): 39.52 (C11), 111.22 (C9′), 117.18 (C7), 118.10 (C2/2′), 125.03 (C3), 134.75 (C8), 141.04 (C1), 146.70 (C4), 152.77 (C10), 157.89 (C6), 165.34 (C5). IR (cm^{-1}): ν (NH): 3388; ν (C=N): 1599; ν_a (NO_2): 1502; ν_s (NO_2): 1324; ν (C–S): 804; ν (Pd–N): 362; ν (Pd–S): 353.

4.3.3. Complex [PdLCl(DMSO)]. A concentrated water solution of LiCl (7.00 mg, 0.165 mmol) was added over a solution of [Pd(L)$_2$] (68.34 mg, 0.086 mmol) in DMSO (20 mL). The solution was stirred at 70 °C for 3 days. The resulting solution was precipitated with distilled water (20 mL), the brown solid was filtered, washed with water and vacuum dried affording 42.54 mg of the product. From a solution in DMSO of the complex, single crystals suitable for structural resolution by SC-XRD were obtained.

[PdLCl(DMSO)]. Brown solid. Yield: 88%. Elemental analysis (wt%) for $C_{18}H_{22}N_5O_3S_2ClPd$: calculated: C, 38.44; H, 3.94; N, 12.45. Experimental: C, 37.87; H, 3.89; N, 12.79. ^{1}H-RMN (300 MHz, DMSO-d_6), δ (ppm): 2.54 (s, H12/12′); 3.07 (s, 6H, H11); 6.76 (d, 2H, H9); 7.75 (d, 2H, H2); 7.96 (d, 2H, H8); 8.22 (d, 2H, H3); 8.30 (s, 1H, H6); 10.30 (s, 1H, N–HA). ^{13}C-RMN (DMSO-d_6), δ (ppm): 39.50 (C11/11′), 40.42 (C12/12′), 111.20 (C9), 117.17 (C7), 118.09 (C2), 124.99 (C3), 134.72 (C8), 141.03 (C1), 146.68 (C4), 152.75 (C10), 157.87 (C6), 165.34 (C5). IR (cm^{-1}): ν (NH): 3222; ν (C=N): 1; ν_a (NO_2): 1503; ν_s (NO_2): 1329; ν (S=O): 1113; ν (C–S): 811; ν (Pd–N): 362; ν (Pd–S): 353; ν (Pd–Cl): 295.

4.4. Crystallography

Data were collected on a Bruker Kappa Apex II diffractometer. A summary of the crystal data, experimental details and refinement results is listed in Table S3.† The software package SHELXTL was used for the space group determination, structure solution, and refinement.[54] The structure was solved by direct methods, completed with difference Fourier syntheses, and refined with anisotropic displacement parameters. All details can be found in CCDC 2119429† which contains the supplementary crystallographic data for this paper.

4.5. Sample preparation in buffer solution of [Pd(L)$_2$] and [PdLCl(DMSO)] complexes

The complexes were initially dissolved in DMSO (5 mM). For all experiments, the desired concentration of complexes was

achieved by dilution of the DMSO stock solution with Tris-HCl aqueous buffer to reach concentration of the complex from 10^{-6}–10^{-4} M. All the solutions and buffers were adjusted to pH 7.2 and 37.0 °C temperature. The studies for [Pd(L)$_2$] and [PdLCl(DMSO)] were performed with 3 and 5% DMSO (v/v) in the final solution.

The temperature stability of the compounds was evaluated by preparing 35 μM samples of each compound in Tris-HCl/NaCl or PBS buffer and recording the absorbance spectrum as the temperature was increased. All the samples had a maximum of 3% (v/v) DMSO in the final solution.

4.6. Spectrophotometric titrations

The spectrophotometric titrations were performed by adding increasing amounts of the corresponding titrant stock solution to the cuvette containing the titrand and recording the absorption or fluorescence spectrum after each addition. Small volumes were precisely measured using a Hamilton glass syringe assembled on a Mitutoyo micrometric screw so that each complete turn of the screw added 8.2 μL (1/50 of a turn was the minimum addition possible). All the spectra were corrected for dilution. Additionally, the fluorescence spectra were corrected for inner-filter effects using eqn (2)

$$F_{corr} = F_{obs} \times 10^{(A_{ex}+A_{em})/2} \quad (2)$$

where A_{ex} and A_{em} are the absorbance values of the sample at the excitation and emission wavelengths, respectively. As the absorbance of DNA, dsRNA and BSA in the spectral range recorded is negligible, A_{ex} and A_{em} were approximated to those of the corresponding complex. Note that, in the calculations, it is considered that we used semi-micro fluorescence cells with an optical path of 1 cm for excitation and 0.2 cm for emission; therefore, it will be $A_{ex} = \varepsilon_{ex} \times C_{complex}$ and $A_{em} = 0.2 \times \varepsilon_{em} \times C_{complex}$.[50,55] Both absorbances were calculated using the molar extinction coefficient (ε) values extracted by the experiment shown in Fig. S5.†

In the EtBr exchange experiments, CT-DNA or dsRNA was first saturated with EtBr, producing the characteristic emission signal of the intercalated probe; then, the molecule to be tested was added to the mixture.

In all the titrations, the DMSO content was kept negligible: the samples had a maximum of 3% DMSO (v/v) in the final solution.

4.7. Electrophoresis assay

Complexes [Pd(L)$_2$] and [PdLCl(DMSO)] were incubated at 37 °C with 0.0625 μg μL^{-1} pBR322 plasmid DNA (only SC form), at different concentrations expressed as r_i = complex : DNA (base pair) ratio. The r_i used is from 0.01 to 0.2, in a total volume of 20 μL. After an incubation period of 24 h, the mobility of the complex-treated pBR322 samples was analyzed by gel electrophoresis at 70 V in Tris/acetate/EDTA buffer. A control of pBR322 was also incubated, and one load of 1 kb ladder was loaded in lane 1 of the gel. The gel was stained with ethidium bromide aqueous solution and DNA bands were visualized with a UV-transilluminator UVITEC Cambridge UVIDOC HD2 instrument. The studies were performed with 1% DMSO (v/v) in the final solution.

4.8. Viscosity

The viscosity experiments were carried out in an automated AND viscometer model SV-1A, at a constant temperature of 25.0 ± 0.1 °C using a water bath with thermostat control. All viscosity assays were carried out using a fixed DNA concentration of 5.69 × 10^{-5} M, with increasing [compound]/[CT-DNA] molar ratios (1/R from 0.0 to 1.0). The temperature was maintained constant at 25.0 ± 0.1 °C using a thermostatic water bath with a water jacket accessory. In all experiments, the desired concentration of each compound was achieved by dilution with Tris-HCl 5 mM/NaCl 100 mM buffer. The samples of the Pd complexes were additionally diluted with DMSO to avoid precipitation, reaching a final DMSO concentration of 3% (v/v). The effect of the addition of the compounds is represented by plotting the CT-DNA relative viscosity, $(\eta/\eta_0)^{1/3}$ against 1/R, where η_0 and η are the relative viscosities of CT-DNA in the absence and presence of the compounds, respectively, and R is the [CT-DNA]/[compound] molar ratio.

4.9. Cell culture and cellular viability (MTT assay)

Human colon (Caco-2, ATCC HTB-37™), prostate (PC-3, ATCC CRL-1435™) carcinoma cell lines and the promyelocytic cell line HL-60 (ATCC®CCL-240TM) were maintained in the DMEM and RPMI medium (last two), respectively, supplemented with glutamax-1 with 10% of heated-inactivated FBS, 1% penicillin/streptomycin, 1% L-glutamine and 1% non-essential amino acids. Both cell lines were routinely grown at 37 °C in a humidified 5% CO_2 atmosphere. Media was changed twice per week and cells were passaged at 80% confluence (cell density at 8 × 10^4, ~1 × 10^5 cells per cm^2), being harvested by trypsinization (1% trypsin–EDTA solution).

The cytotoxic activity of [Pd(L)$_2$] and [PdLCl(DMSO)] complexes, as well as their precursors (86.55 & 60.88% of LH, 13.45 & 18.92% of $K_2[PdCl_4]$, respectively), were analyzed by the colorimetric MTT (3-(4,5-dimethylthiazol-2-yl)-2,5-diphenyltetrazolium bromide) assay. The adherent colon and prostate cell lines (Caco-2 & PC-3 cells) and the suspension HL-60 cells were seeded 72 h prior to the assay in 96-well plates at a density of 1 × 10^5 cells per well in supplemented culture media. The complex suspensions were prepared as a dilution series with cell culture media described as follows: 30 μL of each complex (from a stock prepared at 5% DMSO aqueous solution (v/v)), were added to a final volume of 300 μL per well, yielding different concentrations ranging from 10 to 0.08 μM (in triplicate). Moreover, a set of diverse control wells was left on each plate: (i) medium without cells, (ii) cells with a cytotoxic agent (Triton), (iii) untreated cells and (iv) cells containing medium with the same concentration of DMSO (DMSO control). Subsequently, all these treatments were added to the cells for 72 h, while being maintained at 37 °C under a 5% CO_2 atmosphere.

Cytotoxicity was determined by adding the MTT reactant (0.5 mg mL^{-1} in PBS, incubated at 37 °C for 2 h) followed by

washing with 100 μL of PBS, and ending with the addition of 100 μL of DMSO to each well. Absorbance was determined at λ = 539 nm under stirring. The percentage of cell viability was calculated by the absorbance measurements of control growth and test growth in the presence of the formulations at various concentration levels.

4.10. Cellular uptake

The cells were seeded in 24-well tissue culture plates at a density of 2×10^5 and 4×10^5 cells per well for PC-3 and Caco-2, respectively, and allowed to attach overnight at 37 °C. The adherent cells were incubated with each complex (5 μM) for 72 h at 37 °C. Then, excess complex-solution and dead cells were removed, detaching the adherent cells with trypsin. Cells in the suspension were centrifuged, and the pellets were resuspended in PBS, which was counted and centrifuged (7000 rpm, 5 min, 4 °C). In order to disrupt the cellular membrane, the pellets were suspended in lysis buffer (10 mM Tris, 1.5 mM $MgCl_2$, 140 mM NaCl, pH 8.0–8.3 with 0.02% of Nonidet P40). After 15 min of ice incubation, the suspension was centrifuged at 7000 rpm for 10 min: the nuclear fraction ("pellet") was separated from the cytoplasmic fraction ("supernatant"). The Pd content for complexes $[Pd(L)_2]$, [PdLCl(DMSO)] and its respective controls ($K_2[PdCl_4]$, DMSO control and Pt amount for cisplatin,) in both fractions were measured by ICP-MS. The measurements were made after digestion with ultrapure HNO_3 (65%), H_2O_2 and HCl, followed by evaporation and redissolution of the residue in ultrapure water to obtain a 2.0% (v/v) nitric acid solution, using an ICP-MS NexION 300 PerkinElmer instrument and ^{187}Rhenium as an internal standard.

4.11. Cell Cycle analysis

Caco-2 and PC-3 cells were treated with $[Pd(L)_2]$ and Pd(L)(Cl)(DMSO) (2.5 μM) for 72 h in 96-well plates (at a density of 10×10^4 cells per well). Negative cells (C−: exposed to any treatment) and cisplatin (as reference compound) were included as a control. Cells were trypsinized, harvested and fixed with EtOH (70%), alternating with PBS washing steps. Then, the cells were stained with PI/RNase buffer for 15 min at RT under dark conditions. Finally, the cell cycle distribution was analyzed using flow cytometry (Beckman Coulter: CytoFlex S; λ_{Ex}: 488; λ_{Em}: 585/42 filter).[32,33]

Author contributions

AGQ, TB and PH conceived and designed the research: conceptualization, data curation, methodology, resources, supervision, writing – review & editing. AIM did supervision, methodology and writing & editing. TH, DF and RA conducted the experiments and DF, TH also collaborated in the writing – review & editing.

Conflicts of interest

No conflicts of interest.

Acknowledgements

This contribution is part of the work of CA18202 of the NECTAR Network for Equilibria and Chemical Thermodynamics Advanced Research, supported by the COST (European Cooperation in Science and Technology). AGQ, AIM and DF acknowledge the Spanish MINECO grant PID2019-106220RB100 and MetDrugs Network RED2018-102471T for research discussion. T. B. also thanks CIRCMSB (Consorzio Inter-Universitario di Ricerca in Chimica dei Metalli nei Sistemi Biologici) and CISUP (Centro per la Integrazione della Strumentazione dell'Università di Pisa). T. H. and P. H. acknowledge the "Comunidad de Madrid" and European Regional Development Fund-FEDER 2014-2020-OE REACT-UE 1 for financial support to the VIRMOF-CM project associated with R&D projects in response to COVID-19, the Multifunctional Metallodrugs in Diagnosis and Therapy Network (MICIU, RED2018-102471-T) as well as T.H. thanks to the European Union's Horizon 2020 Research and Innovation Programme under the Marie Sklodowska-Curie grant agreement No 897678 (NeuroMOF). In addition, P. H. acknowledges the Spanish Ramon y Cajal Programme (grant agreement no. 2014 to 16823).

References

1 ECIS - European Cancer Information System, https://ecis.jrc.ec.europa.eu/.
2 Cancer Tomorrow - International Agency for Research on Cancer, World Health Organisation https://gco.iarc.fr/tomorrow/en/.
3 Drugs.com, https://www.drugs.com/pro/cisplatin.html#.
4 Z. Liu and P. J. Sadler, Organoiridium Complexes: Anticancer Agents and Catalysts, *Acc. Chem. Res.*, 2014, **47**, 1174–1185.
5 G. Gupta, P. Kumari, J. Y. Ryu, J. Lee, S. M. Mobin and C. Y. Lee, Mitochondrial Localization of Highly Fluorescent and Photostable BODIPY-Based Ruthenium(II), Rhodium (III), and Iridium(III) Metal Complexes, *Inorg. Chem.*, 2019, **58**, 8587–8595.
6 G. Gupta, S. Cherukommu, G. Srinivas, S. W. Lee, S. H. Mun, J. Jung, N. Nagesh and C. Y. Lee, BODIPY-based Ru(II) and Ir(III) organometallic complexes of avobenzone, a sunscreen material: Potent anticancer agents, *J. Inorg. Biochem.*, 2018, **189**, 17–29.
7 R. P. Paitandi, V. Sharma, V. D. Singh, B. K. Dwivedi, S. M. Mobin and D. S. Pandey, Pyrazole appended quinoline-BODIPY based arene ruthenium complexes: their anticancer activity and potential applications in cellular imaging, *Dalton Trans.*, 2018, **47**, 17500–17514.
8 A. Sengupta, A. Seitz and K. M. Merz, Simulating the Chelate Effect, *J. Am. Chem. Soc.*, 2018, **140**, 15166–15169.
9 Q. Zhao, G. Meng, S. P. Nolan and M. Szostak, N-Heterocyclic Carbene Complexes in C–H Activation Reactions, *Chem. Rev.*, 2020, **120**, 1981–2048.

10 L. Wang, R. Liu, F. Li, Y. Meng and H. Lu, Unveiling the novel characteristics of IGPD polymer and inhibitors binding affinities using 12–6–4 LJ-type nonbonded Mn^{2+} model, *J. Mol. Liq.*, 2021, **322**, 114992.
11 D. Sarko, M. Eisenhut, U. Haberkorn and W. Mier, Bifunctional chelators in the design and application of radiopharmaceuticals for oncological diseases, *Curr. Med. Chem.*, 2012, **19**, 2667–2688.
12 T. Lazarević, A. Rilak and Ž D. Bugarčić, Platinum, palladium, gold and ruthenium complexes as anticancer agents: Current clinical uses, cytotoxicity studies and future perspectives, *Eur. J. Med. Chem.*, 2017, **142**, 8–31.
13 M. Vojtek, M. P. M. Marques, I. M. P. L. V. O. Ferreira, H. Mota-Filipe and C. Diniz, Anticancer activity of palladium-based complexes against triple-negative breast cancer, *Drug Discovery*, 2019, **24**, 1044–1058.
14 European Medicines Agency, **https://www.ema.europa.eu/en/medicines/human/EPAR/tookad**.
15 A. G. Quiroga and C. Navarro Ranninger, Contribution to the SAR field of metallated and coordination complexes: Studies of the palladium and platinum derivatives with selected thiosemicarbazones as antitumoral drugs, *Coord. Chem. Rev.*, 2004, **248**, 119–133.
16 A. I. Matesanz, E. Jimenez-Faraco, M. C. Ruiz, L. M. Balsa, C. Navarro-Ranninger, I. E. León and A. G. Quiroga, Mononuclear Pd(ii) and Pt(ii) complexes with an α-N-heterocyclic thiosemicarbazone: cytotoxicity, solution behaviour and interaction versus proven models from biological media, *Inorg. Chem. Front.*, 2018, **5**, 73–83.
17 M. D. Hall, K. A. Telma, K.-E. Chang, T. D. Lee, J. P. Madigan, J. R. Lloyd, I. S. Goldlust, J. D. Hoeschele and M. M. Gottesman, Say No to DMSO: Dimethylsulfoxide Inactivates Cisplatin, Carboplatin, and Other Platinum Complexes, *Cancer Res.*, 2014, **74**, 3913–3922.
18 M. Patra, T. Joshi, V. Pierroz, K. Ingram, M. Kaiser, S. Ferrari, B. Spingler, J. Keiser and G. Gasser, DMSO-Mediated Ligand Dissociation: Renaissance for Biological Activity of N-Heterocyclic-[Ru(η6-arene)Cl2] Drug Candidates, *Chem. – Eur. J.*, 2013, **19**, 14768–14772.
19 H. P. Varbanov, D. Ortiz, D. Höfer, L. Menin, M. Galanski, B. K. Keppler and P. J. Dyson, Oxaliplatin reacts with DMSO only in the presence of water, *Dalton Trans.*, 2017, **46**, 8929–8932.
20 A. P. Rebolledo, M. Vieites, D. Gambino, O. E. Piro, E. E. Castellano, C. L. Zani, E. M. Souza-Fagundes, L. R. Teixeira, A. A. Batista and H. Beraldo, Palladium(ii) complexes of 2-benzoylpyridine-derived thiosemicarbazones: spectral characterization, structural studies and cytotoxic activity, *J. Inorg. Biochem.*, 2005, **99**, 698–706.
21 A. I. Matesanz, J. Perles and P. Souza, New palladium and platinum complexes with bioactive 3,5-diacetyl-1,2,4-triazol bis(4-cyclohexyl thiosemicarbazone) ligand: chemistry, antiproliferative activity and preliminary toxicity studies, *Dalton Trans.*, 2012, **41**, 12538–12547.
22 L. Fuentes, A. G. Quiroga, J. A. Organero and A. I. Matesanz, Exploring DNA binding ability of two novel α-N-heterocyclic thiosemicarbazone palladium(ii) complexes, *J. Inorg. Biochem.*, 2020, **203**, 110875.
23 F. H. Allen, D. G. Watson, L. Brammer, A. G. Orpen and R. Taylor, in *International Tables for Crystallography*, 2006, pp. 790–811. DOI: **10.1107/97809553602060000621**.
24 R. J. Glisoni, D. A. Chiappetta, L. M. Finkielsztein, A. G. Moglioni and A. Sosnik, Self-aggregation behaviour of novel thiosemicarbazone drug candidates with potential antiviral activity, *New J. Chem.*, 2010, **34**, 2047–2058.
25 E. Ulukaya, F. M. Frame, B. Cevatemre, D. Pellacani, H. Walker, V. M. Mann, M. S. Simms, M. J. Stower, V. T. Yilmaz and N. J. Maitland, Differential Cytotoxic Activity of a Novel Palladium-Based Compound on Prostate Cell Lines, Primary Prostate Epithelial Cells and Prostate Stem Cells, *PLoS One*, 2013, **8**, e64278.
26 J. Morini, G. Babini, S. Barbieri, G. Baiocco and A. Ottolenghi, The Interplay between Radioresistant Caco-2 Cells and the Immune System Increases Epithelial Layer Permeability and Alters Signaling Protein Spectrum, *Front. Immunol.*, 2017, **8**, 1–12.
27 M. Frik, J. Fernández-Gallardo, O. Gonzalo, V. Mangas-Sanjuan, M. González-Alvarez, A. Serrano del Valle, C. Hu, I. González-Alvarez, M. Bermejo, I. Marzo and M. Contel, Cyclometalated Iminophosphorane Gold(iii) and Platinum (ii) Complexes. A Highly Permeable Cationic Platinum(ii) Compound with Promising Anticancer Properties, *J. Med. Chem.*, 2015, **58**, 5825–5841.
28 T. Hidalgo, R. Simón-Vázquez, A. González-Fernández and P. Horcajada, Cracking the immune fingerprint of metal–organic frameworks, *Chem. Sci.*, 2022, **13**, 934–944.
29 S. J. Collins, The HL-60 Promyelocytic Leukemia Cell Line: Proliferation, Differentiation, and Cellular Oncogene Expression, *Blood*, 1987, **70**, 1233–1244.
30 Y. Guo, F. Gao, Q. Wang, K. Wang, S. Pan, Z. Pan, S. Xu, L. Li and D. Zhao, Differentiation of HL-60 cells in serum-free hematopoietic cell media enhances the production of neutrophil extracellular traps, *Exp. Ther. Med.*, 2021, **21**, 353.
31 A. Eastman, Improving anticancer drug development begins with cell culture: misinformation perpetrated by the misuse of cytotoxicity assays, *Oncotarget*, 2016, **8**(5), 8854–8866.
32 N. C. de Carvalho, S. P. Neves, R. B. Dias, L. d. F. Valverde, C. B. S. Sales, C. A. G. Rocha, M. B. P. Soares, E. R. dos Santos, R. M. M. Oliveira, R. M. Carlos, P. C. L. Nogueira and D. P. Bezerra, A novel ruthenium complex with xanthoxylin induces S-phase arrest and causes ERK1/2-mediated apoptosis in HepG2 cells through a p53-independent pathway, *Cell Death Dis.*, 2018, **9**, 79.
33 N. Kuwajerwala, E. Cifuentes, S. Gautam, M. Menon, E. R. Barrack and G. P. V. Reddy, Resveratrol Induces Prostate Cancer Cell Entry into S Phase and Inhibits DNA Synthesis, *Cancer Res.*, 2002, **62**, 2488–2492.
34 R. Czarnomysy, D. Radomska, O. K. Szewczyk, P. Roszczenko and K. Bielawski, Platinum and Palladium Complexes as Promising Sources for Antitumor Treatments, *Int. J. Mol. Sci.*, 2021, **22**, 8271.

35 A. Ruszkowska, M. Ruszkowski, J. P. Hulewicz, Z. Dauter and J. A. Brown, Molecular structure of a U·A-U-rich RNA triple helix with 11 consecutive base triples, *Nucleic Acids Res.*, 2020, **48**, 3304–3314.

36 C. A. Theimer, C. A. Blois and J. Feigon, Structure of the Human Telomerase RNA Pseudoknot Reveals Conserved Tertiary Interactions Essential for Function, *Mol. Cell*, 2005, **17**, 671–682.

37 M. Mitton-Fry Rachel, J. DeGregorio Suzanne, J. Wang, A. Steitz Thomas and A. Steitz Joan, Poly(A) Tail Recognition by a Viral RNA Element Through Assembly of a Triple Helix, *Science*, 2010, **330**, 1244–1247.

38 L. Huang and D. M. J. Lilley, Structure and ligand binding of the SAM-V riboswitch, *Nucleic Acids Res.*, 2018, **46**, 6869–6879.

39 F. Binacchi, F. Guarra, D. Cirri, T. Marzo, A. Pratesi, L. Messori, C. Gabbiani and T. Biver, On the Different Mode of Action of Au(I)/Ag(I)-NHC Bis-Anthracenyl Complexes Towards Selected Target Biomolecules, *Molecules*, 2020, **25**, 5446.

40 M. N. Patel, P. A. Dosi and B. S. Bhatt, Square planar palladium(II) complexes of bipyridines: synthesis, characterization, and biological studies, *J. Coord. Chem.*, 2012, **65**, 3833–3844.

41 F. Macii, R. Detti, F. R. Bloise, S. Giannarelli and T. Biver, Spectroscopic Analysis of the Binding of Paraquat and Diquat Herbicides to Biosubstrates, *Int. J. Environ. Res. Public Health*, 2021, **18**, 2412.

42 N. Korkmaz, A. Aydın, A. Karadağ, Y. Yanar, Y. Maaşoğlu, E. Şahin and Ş. Tekin, New bimetallic dicyanidoargentate (I)-based coordination compounds: Synthesis, characterization, biological activities and DNA-BSA binding affinities, *Spectrochim. Acta, Part A*, 2017, **173**, 1007–1022.

43 A. Kellett, Z. Molphy, C. Slator, V. McKee and N. P. Farrell, Molecular methods for assessment of non-covalent metallodrug–DNA interactions, *Chem. Soc. Rev.*, 2019, **48**, 971–988.

44 A. G. Quiroga, J. M. Pérez, I. López-Solera, J. R. Masaguer, A. Luque, P. Román, A. Edwards, C. Alonso and C. Navarro-Ranninger, Novel Tetranuclear Orthometalated Complexes of Pd(II) and Pt(II) Derived from p-Isopropylbenzaldehyde Thiosemicarbazone with Cytotoxic Activity in cis-DDP Resistant Tumor Cell Lines. Interaction of These Complexes with DNA, *J. Med. Chem.*, 1998, **41**, 1399–1408.

45 S. Cabrera, F. Navas, A. I. Matesanz, M. Maroto, T. Riedel, P. J. Dyson and A. G. Quiroga, Versatile Route to trans-Platinum(II) Complexes via Manipulation of a Coordinated 3-(Pyridin-3-yl)propanoic Acid Ligand, *Inorg. Chem.*, 2019, **58**, 7200–7208.

46 E. R. Jamieson and S. J. Lippard, Structure, Recognition, and Processing of Cisplatin–DNA Adducts, *Chem. Rev.*, 1999, **99**, 2467–2498.

47 G. L. Cohen, W. R. Bauer, J. K. Barton and S. J. Lippard, Binding of cis- and trans-dichlorodiammineplatinum(II) to DNA: evidence for unwinding and shortening of the double helix, *Science*, 1979, **203**, 1014–1016.

48 Y. Zhang, J. Pan, G. Zhang and X. Zhou, Intercalation of herbicide propyzamide into DNA using acridine orange as a fluorescence probe, *Sens. Actuators, B*, 2015, **206**, 630–639.

49 A. I. Matesanz, P. Albacete, J. Perles and P. Souza, A structural and biological study on the new 3,5-diacetyl-1,2,4-triazol bis(p-chlorophenylthiosemicarbazone) ligand and its bimetallic complexes, *Inorg. Chem. Front.*, 2015, **2**, 75–84.

50 F. Macii and T. Biver, Spectrofluorimetric analysis of the binding of a target molecule to serum albumin: tricky aspects and tips, *J. Inorg. Biochem.*, 2021, **216**, 111305.

51 T. Tŏpala, A. Pascual-Álvarez, M. Moldes-Tolosa, A. Bodoki, A. Castiñeiras, J. Torres, C. Del Pozo, J. Borrás and G. Alzuet-Piña, New sulfonamide complexes with essential metal ions [Cu(II), Co(II), Ni(II) and Zn(II)]. Effect of the geometry and the metal ion on DNA binding and nuclease activity. BSA protein interaction, *J. Inorg. Biochem.*, 2020, **202**, 110823.

52 B. Elsadek and F. Kratz, Impact of albumin on drug delivery—New applications on the horizon, *J. Controlled Release*, 2012, **157**, 4–28.

53 R. A. Gossage, H. A. Jenkins, N. D. Jones, R. C. Jones and B. F. Yates, Pre-catalyst resting states: a kinetic, thermodynamic and quantum mechanical analyses of [PdCl2(2-oxazoline)2] complexes, *Dalton Trans.*, 2008, 3115–3122, DOI: **10.1039/B801951G**.

54 SHELXTL Version 2014/7, **https://shelx.uni-ac.gwdg.de/SHELX/index.php**.

55 M. van de Weert and L. Stella, Fluorescence quenching and ligand binding: A critical discussion of a popular methodology, *J. Mol. Struct.*, 2011, **998**, 144–150.

